14-3-3 regulation of Ncd reveals a new mechanism for targeting 4 proteins to the spindle in oocytes

14-3-3 regulation of Ncd reveals a new mechanism for targeting proteins to the spindle in oocytes

Robin Beaven[1,5], Ricardo Nunes Bastos[1], Christos Spanos[1], Pierre Romé[2,6], C. Fiona Cullen[1], Juri Rappsilber[1,3], Régis Giet[2], Gohta Goshima[4] and Hiroyuki Ohkura[1]

1. Wellcome Centre for Cell Biology, School of Biological Sciences, University of Edinburgh, Edinburgh EH9 3BF, UK
2. Institut de Génétique et Développement de Rennes-Université de Rennes I-CNRS- UMR 6290, Rennes Cedex, France.
3. Chair of Bioanalytics, Institute of Biotechnology, Technische Universität Berlin, Berlin, 13355, Germany
4. Division of Biological Science, Graduate School of Science, Nagoya University, Furo-cho, Chikusa-ku, Nagoya 464-8602, Japan
5. present address: Centre for Integrative Physiology, Edinburgh Medical School, University of Edinburgh, Edinburgh EH8 9XD, UK
6. present address: Wellcome Centre for Cell Biology, University of Edinburgh, Edinburgh EH9 3BF, UK

14-3-3 interacts with the kinesin-14 Ncd and prevents it from binding microtubules. Aurora B provides a spatial cue which releases Ncd from 14-3-3 around chromosomes, allowing Ncd to selectively bind the spindle microtubules in the large volume of oocytes.

Abstract

The meiotic spindle is formed without centrosomes in a large volume of oocytes. Local activation of crucial spindle proteins around chromosomes is important for formation and maintenance of a bipolar spindle in oocytes. We found that the phospho-docking 14-3-3 proteins stabilise spindle bipolarity in *Drosophila* oocytes. A critical 14-3-3 target is the minus-end directed motor Ncd (human HSET; kinesin-14) which has well documented roles in stabilising a bipolar spindle in oocytes. Phospho-docking by 14-3-3 inhibits the microtubule binding activity of the non-motor Ncd tail. Further phosphorylation by Aurora B kinase can release Ncd from this inhibitory effect of 14-3-3. As Aurora B localises to chromosomes and spindles, 14-3-3 facilitates specific association of Ncd with spindle microtubules by preventing Ncd from binding to non-spindle microtubules in oocytes. Therefore, 14-3-3 translates a spatial cue provided by Aurora B to target Ncd selectively to the spindle within the large volume of oocytes.

Introduction

Meiotic spindle formation in oocytes faces two challenges, lack of centrosomes and a large cytoplasmic volume in oocytes (Ohkura, 2015). Spatial regulation of motor and non-motor microtubule-associated proteins (MAPs) is crucial to overcome these challenges. Furthermore, multiple kinases are important for spindle assembly and organisation in oocytes (Sampath et al., 2004; Tseng et al., 2010; Colombié et al., 2008; Radford et al., 2012b; Swain et al., 2008; Sumiyoshi et al., 2015; Pearson et al., 2005; Loh et al., 2012), but little is understood of how they regulate a meiotic spindle. It has been proposed that, in addition to Ran, chromatin-bound Aurora B provides a critical spatial cue for bipolar spindle assembly in oocytes (Sampath et al., 2004; Colombié et al., 2008; Radford et al., 2012b), but little is yet known about how this signal is translated into spindle morphogenesis, except that it inhibits the microtubule depolymerase kinesin-13 (Ohi et al., 2004).

14-3-3 phospho-docking proteins sit at the core of many phospho-regulatory pathways, and can act as integrators of different pathways (Morrison, 2009; Gardino and Yaffe, 2011). 14-3-3 proteins bind phospho-proteins and change their activity, localisation or protein interaction. *Drosophila* has only two 14-3-3 isoforms, ε and ζ, compared to the seven vertebrate isoforms which frequently act redundantly (Darling et al., 2005). *Drosophila* therefore provides an advantage in defining *in vivo* roles of 14-3-3. It has revealed roles in development (Chang and Rubin, 1997; Kockel et al., 1997; Benton et al., 2002), but a role in the meiotic spindles has not been established before.

Here we report that 14-3-3 is important for maintaining a bipolar spindle in oocytes. 14-3-3 interacts with the kinesin-14 Ncd and prevents it from binding to microtubules, but further phosphorylation by Aurora B releases Ncd from 14-3-3 to allow Ncd binding to microtubules. In response to the spatial cue provided by Aurora B, 14-3-3 promotes Ncd binding specifically to spindle microtubules by preventing it from binding other microtubules in the large cytoplasmic volume of oocytes.

Results and Discussion

14-3-3 regulates the meiotic spindle in oocytes

To test a potential function of 14-3-3ε in meiotic spindle organisation, we immunostained mature oocytes that naturally arrest in metaphase I. Depletion of 14-3-3ε by expressing either of two non-overlapping short-hairpin RNAs (shRNAs) in the female germline resulted in similar abnormal spindle morphologies (**Fig 1A-C,S1)**. Interestingly, in S2 cells, 14-3-3ε has no significant roles in the morphology of mitotic spindles both in the presence or absence of centrosomes (Goshima et al., 2007; Moutinho-Pereira et al., 2013).

In contrast to 14-3-3ε, depletion of the other isoform 14-3-3ζ in oocytes showed no spindle organisation defects (**Fig 1A**). Furthermore, 14-3-3ε depletion led to female sterility, while 14-3-3ζ depletion did not. Co-depletion of 14-3-3ε and ζ led to a more severe spindle defect than loss of 14-3-3ε alone (**Fig 1A**), demonstrating that the two 14-3-3 isoforms together regulate the meiotic spindle with 14-3-3ε playing the major role.

14-3-3 maintains the bipolarity of the acentrosomal spindle in oocytes

To define the role of 14-3-3 in the meiotic spindle, matured control or 14-3-3ε RNAi oocytes were immunostained. In control, we typically observed a bipolar metaphase I spindle with focused poles (**Fig 1A-C**). In contrast, 14-3-3ε depleted oocytes had abnormal spindles most typically tripolar or with unfocused poles (**Fig 1A-C**). The localisation of the pole protein TACC and the equator protein Subito/MKlp2 were not altered (**Fig 1B**), suggesting that the spindle bipolarity is specifically altered. In contrast, the crucial microtubule regulator Msps (the XMAP215/TOG orthologue) that normally accumulates at the spindle poles was more often observed at the spindle equator upon 14-3-3ε depletion (**Fig 1C**). Interestingly, we previously found that a hypomorphic *msps* mutant showed a tripolar meiotic spindle morphology (Cullen and Ohkura, 2001) similar to that seen upon 14-3-3ε depletion. Compromised Msps localisation is therefore likely to contribute to the spindle defect seen in 14-3-3ε depleted oocytes.

Next, to determine whether 14-3-3ε is required for the stability of spindle bipolarity, we imaged live metaphase I oocytes expressing GFP-α-tubulin. In control, all bipolar spindles stably retained their organisation (**Fig 1D**) (Colombié et al., 2008). In contrast, 35% of 14-3-3ε RNAi spindles changed their morphology during the imaging for an average of 39 minutes each. In some cases, a bipolar spindle became tripolar, or a tripolar spindle became bipolar. In other cases, more complex morphological changes were involved (**Fig 1D**). This revealed the important role of 14-3-3ε for the stability of bipolar spindles in oocytes.

14-3-3 interacts with the kinesin-14 Ncd

To identify potential binding partners of 14-3-3, we used recombinant GST-14-3-3ε for pull-down from ovary or S2 cultured cell extract. Mass-spectrometry of these fractions and controls identified potential binding partners including previously known 14-3-3 partners such as Par-1 and Bazooka (Benton et al., 2002; Benton and St Johnston, 2003) (**Table S1**). 14-3-3ζ was also identified, suggesting hetero-dimer formation.

In addition, previously unreported 14-3-3 partners were identified, including the kinesin-14 Ncd. Our immunoblotting confirmed that endogenous Ncd protein was pulled down by the GST-14-3-3ε from ovaries, but not by the GST control (**Fig 2A**). Ncd is important for stabilising the bipolar spindle in oocytes (Kimble and Church, 1983; Hatsumi and Endow, 1992; Matthies et al., 1996), and also for efficient localisation of Msps to the poles (Cullen and Ohkura, 2001). As described above, 14-3-3ε depletion resulted in compromised Msps pole localisation and similar spindle defects to a hypomorphic *msps* mutant. Therefore we hypothesised that 14-3-3 interaction with Ncd is important for stabilising spindle bipolarity in oocytes.

To specifically disrupt the 14-3-3-Ncd interaction, we determined the interaction sites on Ncd. Bioinformatics analysis identified S96 as the site that best fits the consensus (RxxpS/pTxP; Johnson et al., 2010), and S79 and S114 as sites that fit with low stringency. All three sites are located in the non-motor tail region of Ncd (**Fig 2B**). Previous global

phospho-proteomics analyses (Zai et al., 2008; Hilger et al., 2009; Bodenmiller et al., 2007) showed that all three sites are indeed phosphorylated in *Drosophila*.

To test the requirements of these sites for 14-3-3 binding, we made non-phosphorylatable alanine mutations of the best predicted site alone, Ncd(S96A), or of all three sites, Ncd-3xA. We first tested whether these mutations disrupt interaction with 14-3-3ε using S2 cells. We depleted the endogenous Ncd by RNAi and transiently expressed GFP-tagged wild-type or mutant Ncd resistant to RNAi. The amount of Ncd pulled down with GST-14-3-3ε was drastically reduced for Ncd(S96A) compared to wild-type Ncd, with Ncd-3xA giving minimal binding (**Fig 2C**). We conclude that phospho-S96 is a critical binding site for 14-3-3ε, although phospho-S79 and phospho-S114 may facilitate some residual binding.

14-3-3 binding promotes spindle association and function of Ncd in oocytes

To test for a role of 14-3-3-Ncd interaction, we expressed Ncd(96A) in an *ncd* null mutant (*ncd*^{1}) background. It has previously been shown that expression of Ncd-GFP from the native *ncd* promoter can rescue the meiotic spindle phenotype observed in the *ncd* null mutant (Endow and Komma, 1997). We therefore generated transgenic flies expressing Ncd-GFP with or without the S96A mutation under the native *ncd* promoter. We noticed a reduction in the protein levels for Ncd(S96A) compared to that of the wild-type form. To compensate for this, we compared one copy of the wild-type transgene with two copies of the mutant transgene, which gave comparable protein levels (**Fig S1B**).

The spindle signal of Ncd(S96A)-GFP, relative to the α-tubulin signal, was dramatically reduced compared to Ncd-GFP (**Fig 2D,E**), even when comparable amounts were expressed (**Fig S1B**). Consistent with these observations, 14-3-3 depleted oocytes also have a reduced Ncd protein level and localisation on the meiotic spindle (**Fig S1C-F**). Taken together, we conclude that 14-3-3 binding to phospho-S96 of Ncd is essential for efficient association of Ncd with the meiotic spindle in oocytes.

In the *ncd* mutant without any transgenes, we observed highly frequent spindle abnormalities, including spindles with multiple poles or unfocused poles (**Fig 2D,F**), as previously described (Kimble and Church, 1983; Hatsumi and Endow, 1992; Matthies et al.,

1996). The wild-type Ncd-GFP transgene restored spindle bipolarity, while Ncd(S96A)-GFP transgene did not rescue these spindle abnormalities (**Fig 2D,F**). These observations demonstrated that 14-3-3 binding to phospho-S96 of Ncd is essential for efficient Ncd association with the meiotic spindle, and its function in organising the meiotic spindle.

14-3-3 interaction suppresses binding of Ncd to microtubules *in vitro*

S96 of Ncd lies within a microtubule-binding region of the non-motor tail of Ncd (**Fig 2B**; Karabay and Walker, 1999). This microtubule-binding activity of the Ncd tail is thought to be important for cross-linking parallel microtubules to focus spindle poles in oocytes (Sköld et al., 2005). Therefore, we hypothesised that 14-3-3 binding may enhance the microtubule binding activity of the Ncd tail.

To test this hypothesis biochemically, we first confirmed that 14-3-3ε can directly bind phospho-S96 of Ncd *in vitro*. We expressed and purified a GST-fused wild-type Ncd tail fragment (amino acids 58-192) and non-phosphorylatable Ncd(S96A) in bacteria. To phosphorylate Ncd at S96 *in vitro*, we tested commercially available protein kinases, human PKD2 and CAMK2, predicted to phosphorylate S96. We found that PKD2, but not CAMK2, can phosphorylate the Ncd tail fragment specifically at S96 *in vitro* (**Fig 3A**). We also generated a phospho-specific antibody against phospho-S96, and showed that 14-3-3ε specifically and efficiently pulled down the phosphorylated Ncd tail, confirming that 14-3-3ε binds to phospho-S96 (**Fig 3B**).

Next we examined whether 14-3-3ε binding increases the microtubule binding activity of Ncd *in vitro* (**Fig 3C**). Purified Ncd tail was fully phosphorylated by PKD2, and then incubated with microtubules pre-polymerised from porcine brain tubulin in the presence and absence of 14-3-3ε. After centrifugation, the microtubule fraction (pellet) and the supernatant were analysed by Coomassie staining and immunoblotting using the phospho-specific Ncd(pS96) antibody.

To our surprise, we found that 14-3-3ε drastically reduced the microtubule binding activity of Ncd phosphorylated at S96 by PKD2 (**Fig 3D,S2**). Controls (either S96 phosphorylation alone or the presence of 14-3-3ε alone) did not alter the microtubule binding

activity of this Ncd tail fragment (**Fig 3D,S2**). We therefore conclude that phospho-dependent binding of 14-3-3ε to Ncd suppresses microtubule binding, rather than enhancing it, which is in apparent contradiction to our above cytological observation. To confirm that phosphorylation of S96, not other sites, is responsible for this reduction, the same experiment was carried out using the fragment carrying the S96A mutation. The S96A mutation on its own or together with PKD2 incubation did not alter the microtubule binding or solubility of this mutant fragment in the presence or absence of 14-3-3ε (**Fig 3D,S2**). This confirms that phosphorylation at S96 is required for the suppression of the microtubule binding activity by 14-3-3.

Aurora B releases Ncd from 14-3-3ε to restore the microtubule binding activity of Ncd

14-3-3 binding suppresses microtubule binding activity of Ncd *in vitro*, while our cytological study showed that 14-3-3 binding promotes Ncd association with the meiotic spindle in oocytes. A key to reconcile these apparently contradictory findings could lie in the observation that the large cytoplasmic volume of oocytes contains numerous non-spindle microtubules (Radford et al., 2012a), which potentially compete with spindle microtubules for binding of MAPs. We hypothesise that 14-3-3 binding suppresses the interaction of Ncd with non-spindle microtubules, but this 14-3-3 binding is prevented around chromosomes to allow selective interaction of Ncd with spindle microtubules (**Fig 5D**). Without 14-3-3 binding, most Ncd is non-selectively bound and sequestered by numerous non-spindle microtubules in oocytes, resulting in reduced Ncd association with spindle microtubules.

Visual inspection of the Ncd sequence identified a serine (S94) near S96 (**Fig 2B**). This S94 has been shown to be phosphorylated in *Drosophila* (Zai et al., 2008; Hilger et al., 2009; Bodenmiller et al., 2007), and is potentially phosphorylated by Aurora A/B. We hypothesise that 14-3-3 binding to Ncd is blocked by phosphorylation at S94 by Aurora B, which localises to the chromosome/kinetochores and the spindle midzone in oocytes (Colombié et al., 2008; Radford et al., 2012b). Thus this could provide a mechanism to allow Ncd to selectively associate with spindle microtubules around chromosomes.

To test this hypothesis, we first expressed GFP-tagged wild-type Ncd, non-phosphorylatable Ncd(S94A) and phospho-mimetic Ncd(S94D) in S2 cells depleted of endogenous Ncd. Ncd and Ncd(S94A) were efficiently pulled down with 14-3-3ε, while the phospho-mimetic Ncd(S94D) was not (**Fig 4A**). This suggests that phosphorylation of S94 can prevent 14-3-3ε binding to Ncd.

To test whether Aurora B can phosphorylate Ncd *in vitro*, we incubated the Ncd tail fragment with Aurora B (and/or PKD2). Mobility shifts on a phosphate-affinity (PhosTag) polyacrylamide gel demonstrated that Aurora B phosphorylated the Ncd tail fragment in addition to PKD2 phosphorylation (**Fig 4B**).

To determine the effect of Aurora B phosphorylation on Ncd *in vitro*, the Ncd tails phosphorylated using these different conditions were tested for interaction with 14-3-3ε or microtubules. Ncd interacted with 14-3-3ε when S96 was phosphorylated, but additional phosphorylation at S94 by Aurora B prevented the interaction (**Fig 4C**). Without phosphorylation, the Ncd tail interacted with microtubules, and S96 phosphorylation by PKD2 inhibited this interaction in the presence of 14-3-3ε, as we previously observed. Further Aurora B phosphorylation restored microtubule binding of phosphorylated Ncd at S96. Aurora B phosphorylation alone slightly reduced the microtubule binding activity of Ncd independently of 14-3-3ε (**Fig 4D,S3**). These results demonstrated that Aurora B phosphorylation can release Ncd phosphorylated at S96 from the inhibitory effect of 14-3-3ε to allow binding to microtubules.

Phosphorylation of putative Aurora B site is important for spindle targeting and function of Ncd in oocytes

To test the importance of Aurora B phosphorylation of Ncd at S94 in oocytes, we expressed wild-type Ncd and non-phosphorylatable Ncd(S94A) in the *ncd* null mutant. The Ncd(S94A)-GFP signal was dramatically reduced on the spindle when compared to the wild-type version (**Fig 5A,B**), when comparable amounts of protein were expressed (**Fig S1B**). Ncd(S94A)-GFP showed slightly higher residual signal than Ncd(S96A)-GFP, suggesting additional S94-independent regulation. Furthermore, the Ncd(S94A)-GFP transgene did not rescue the

spindle abnormalities in the *ncd* null mutant (**Fig 5A,C**). These observations demonstrate that phosphorylation of Ncd at S94 is essential for its efficient spindle association and function in organising the meiotic spindle.

14-3-3 reads the Aurora B spatial cue to selectively target Ncd to the meiotic spindle

Our study has identified a novel mechanism that targets a protein to the meiotic spindle in the large volume of oocytes. 14-3-3 cooperates with Aurora B to target the kinesin-14 Ncd to the meiotic spindle by suppressing binding to non-spindle microtubules (**Fig 5D**).

As oocytes lack centrosomes and are exceptionally large, it is crucial to locally activate the factors important for bipolar spindle formation in response to spatial cues provided by chromosomes. Mainly using *Xenopus* egg extract, the role of the Ran-importin pathway is well described in this context (Kalab et al., 1999; Carazo-Salas et al., 1999; Ohba et al., 1999; Wilde and Zheng, 1999; Gruss et al., 2001; Nachury et al., 2001; Wiese et al., 2001). Importin binds and inhibits proteins collectively called spindle assembly factors (SAFs), and chromatin-bound Ran-GEF produces a localised signal, Ran-GTP, which releases SAFs from the inhibitory effects of importin (**Fig 5E**). However, evidence from living mouse and *Drosophila* oocytes suggested the presence of a pathway alternative to Ran-importin (Dumont et al., 2007; Cerario and McKim, 2011). Other studies indicated that chromatin-bound Aurora B is providing a crucial spatial cue in oocytes (Sampath et al., 2004; Colombié et al., 2008; Radford et al., 2012b). How this Aurora B spatial cue translates into local activation of spindle proteins has remained unclear.

Our study uncovered the Aurora B-14-3-3 pathway that acts analogously to the Ran-Importin pathway (**Fig 5E**). Away from chromosomes, in a role similar to that of importin, 14-3-3 binds to and inhibits Ncd. Near chromosomes, instead of Ran-GTP, chromatin-bound Aurora B phosphorylates and releases Ncd from the inhibitory effects of 14-3-3. Our study therefore provides a new conceptual framework of how the chromosomal spatial cue is translated into spindle morphogenesis in oocytes.

Evidence suggests that this role of the Aurora B-14-3-3 pathway may be conserved also in mammalian oocytes and that Ncd may not be the only target. Depletion of the mouse

14-3-3η in oocytes results in spindle disorganisation (De and Kline, 2013). In mitotic anaphase/telophase mammalian cells, the kinesin-6 MKlp1 is regulated by a similar mechanism (Douglas et al., 2010), which is potentially used also in oocytes. Therefore, the Aurora B-14-3-3 pathway is likely to provide a general and conserved mechanism to locally activate spindle proteins in the large volume of oocytes.

Materials and Methods

Drosophila genetics

Standard fly techniques were used (Ashburner et al., 2005). Control were wild type (w^{1118}) or flies expressing shRNA against white gene (GL00094) driven using the same driver as in experimental conditions. The following shRNA lines were used: 14-3-3ε line 1 (GL00366), 14-3-3ε line 2 (HMS01229) and 14-3-3ζ (GL01310). The two 14-3-3ε lines gave comparable results (Fig. S1) and were used interchangeably. GAL4 driver lines used were V2H (P{MatTubulin67C-Gal4}V2H), V37 (P{MatTubulin67C-Gal4}V37), and maternal double driver (MDD) (P{GAL4-nos.NGT}40; P{GAL4::VP16-nos.UTR}MVD1). UASp-GFP-α-tubulin, recombined with V37, was used for live imaging of the meiotic spindle. For removal of endogenous Ncd in oocytes, flies homozygous for the ncd^1 null allele, or carrying the ncd^1 allele over a deficiency (*Df(3R)BSC547*) uncovering *ncd* were used. These two conditions gave comparable results (Fig. S1) and were used interchangeably. To generate transgenic flies for *ncd-GFP* variants, phiC31 integrase-mediated transgenesis onto the 3rd chromosome was performed by BestGene Inc, using the VK33 site in the strain BL9750.

Cytology and image analysis

To obtain oocytes, freshly eclosed females were matured at 25°C for 3-5 days on yeasted food, in the presence of males. For fixed analysis samples were dissected in methanol and stained as previously described (Cullen and Ohkura, 2001). Under these conditions, large oocytes consisted mostly of those at stage 14 that naturally arrest in metaphase I. The following primary antibodies were used for immunostaining: anti-α-tubulin (mouse monoclonal DM1A; 1:250; Sigma), anti-TACC (rabbit polyclonal D-TACC-CTD; 1:1000, Loh et al., 2012), anti-Subito (rat polyclonal; 1:250; Loh et al., 2012), anti-Msps (rabbit polyclonal; HN264, 1:250, Cullen and Ohkura, 2001), anti-Ncd (rabbit polyclonal, 1:1,000, this study) and anti-GFP (rabbit polyclonal; A11122, 1:500 for Fig. 2 or 1:250 for Fig. 5, Thermo Fisher Scientific). Cy3, Cy5 or Alexa488 conjugated secondary antibodies were used (1:250-

1:1000, Jackson Lab or Molecular Probes) and DNA was stained using 0.4 µg/ml DAPI (Sigma).

Fixed oocytes were imaged as described in Głuszek et al. (2015) using an Axioimager (Zeiss) attached to LSM510Exciter (Zeiss) for Fig. 1, 2, S1 (except the last two of S1A) or to LSM800 (Zeiss) for Fig. 5 (and the last two of Fig.S1A). Live imaging was performed on a spinning disk confocal microscope as described in (Głuszek et al., 2015). Z-sections were taken at 0.8 µm at 1 min intervals and maximum intensity projections are displayed.

For Fig. 2 and 5, the total signal intensities of tubulin and Ncd on the spindle were estimated using the following formulas. Two areas (L, S) were drawn on the maximum intensity projection made from Z-series of images. Area L includes the spindle and surrounding region, and Area S includes mainly the spindle.

$[I_S-N_S*(I_L-I_S)/(N_L-N_S)]/[(I_L-I_S)/(N_L-N_S)]$

where I and N are the total pixel intensity and pixel number in the specified area, respectively.

To measure the signal intensities of Ncd and α-tubulin along the spindle for Fig. S1, images were taken using identical settings and maximum intensity projections generated. For each spindle a line was drawn along the spindle length, avoiding the region where microtubules are excluded by the chromosomes, using the segmented line tool of ImageJ. The grey values of both channels were taken for pixels along the line. A mean background grey value was calculated for each channel from an equal sized area adjacent to the spindle, and this was subtracted from each value, before the Ncd/Tubulin intensity values were calculated. These were used to generate a mean value for each spindle. All spindle values were normalised to the median control value in each experiment. To give an idea of staining distribution, pixel intensity data was grouped into 50 sections running from one pole to the other, and mean values were generated for each group. These 50 positions were taken as normalised spindle positions, the values from which could then be averaged for the whole set of spindles for each treatment.

p-values were calculated using χ^2 tests (in the cases of Fig. 1A,2F,5C, the proportion of bipolar to non-bipolar spindles was used) except for Fig. 2E,5B,S1D where the Wilcoxon-ranked sum test was used.

Molecular techniques

Entry plasmids were generated for use with the gateway cloning system, by PCR amplifying the desired fragment and introducing into the pENTR vector using the pENTR Directional Cloning kit, following the manufacturer's instructions (Invitrogen). To generate the Ncd entry plasmid (Ncd pENTR), the Ncd coding region without the stop codon was amplified from cDNA (LD29131). S96A mutation, S94D mutation, S94D mutation and S79A/S96A/S114A triple mutations (3xA) were introduced by PCR-amplifying *ncd* fragments using overlapping mutation-bearing primers and joining the PCR products (NEB) using Gibson assembly. Mutated plasmids were sequenced to confirm no undesired mutations.

Inserts in the pENTR vector were transferred to the desired destination vector using the LR recombination reaction following manufacturer's instructions (Invitrogen). For expression constructs, appropriate destination vectors from the Drosophila Gateway vector collection made by Dr Murphy (generated by T. Murphy's laboratory, Carnegie Institution of Washington) were used. The ϕPGW and ϕPWG destination vectors are modified versions of the pPGW Gateway vector into which *attB* has been inserted, for PhiC31 integrase-mediated transgenesis.

Transgenic constructs carrying *ncd* variants with the endogenous ncd promoter were generated as follows. Sap I sites and additional sequences were added using PCR to both ends of the genomic region containing the 2.8 kb *ncd* upstream region and the 5' end of the coding region of *ncd*. The additional sequences were designed to have overlaps with the ends of EcoRI/StuI-digested ϕPWG inserted with the *ncd* coding region. Therefore the SapI-digested *ncd* promoter fragment was able to be joined together with the EcoRI/StuI-digested *ncd*-coding region in ϕPWG by Gibson assembly.

For RNAi in S2 cells, templates for dsRNA synthesis were amplified using the following primers and a second PCR step was used to add the full T7 promoter. *ncd* UTRs (CGACTCACTATAGGGAGACCGTACTCTCCCGACAAATGG and CGACTCACTATAGGGAGACATCGCCAACTGTGTTGTGCC, CGACTCACTATAGGGAGATGCATTCTGAGCCCAGTT and CGACTCACTATAGGGAGATTTAGCTTTGAATTCCAGCAC).

GST-Ncd(58-192) in pGEX-6p-2 was used for bacterial expression. The S96A mutation was introduced into this plasmid as described above. The coding sequences from 14-3-3ε cDNA (MIP08648) was cloned into pENTR and then transferred into the pMTWG, pMAL-c2 and pGEX-4T1 destination vectors.

Protein expression in bacteria and antibodies

For bacterial expression of proteins, bacteria were cultured overnight at 18°C in the presence of 1 mM IPTG. For expression of GST-Ncd(58-192), 0.5 mM IPTG was used and pellets were frozen and stored at -80°C. To generate the Ncd antibody (Ncd 067), Tail-Ncd-His_6 and Stalk-Ncd-His_6 were purified as described before (Giet et al., 2002). Proteins were expressed in *E. coli* BL21(DE3) pLysS for 4 h at 25°C, purified on a nickel column , then dialysed against PBS. Both purified Tail-Ncd-His_6 and Stalk-Ncd-His_6 proteins were mixed to immunise a rabbit. A phospho-specific antibody designed to recognise pS96-Ncd was generated in rat by Eurogentec, using the peptide (KLRRSRpSACDIN) coupled to the carrier on the N-term, as the antigen.

The following primary antibodies were used: anti-GFP (rabbit, 1:1000, A11122, Thermo Fisher Scientific), anti-Ncd (rabbit, 1:1,000, this study), anti-pS96-Ncd (rat, 1:1,000, this study). Secondary antibodies were either from Licor, visualised on Licor Odyssey scanner (v3.0.30), except for right panel of Figure 3B in which HRP labelled antibodies (Jackson labs) were used and detected by ECL Western Blotting Detection Reagent (Amersham) and films following manufacturer's instructions.

GST-14-3-3ε pull-down assay from S2 cell or ovary extract

For GST-14-3-3ε pulldown, bacteria expressing GST-14-3-3ε or GST control were sonicated in PBS + 1% Triton X-100 + protease inhibitor (complete Mini Protease Inhibitor Cocktail Tablets, Roche), and centrifuged down at 13,000 rpm, 12 min, 4°C. Supernatant was incubated on spinner at 4°C with washed glutathione-sepharose beads. Beads subsequently washed 3 times in lysis buffer (25 mM Tris pH 7.6, 50 mM NaCl, 1 mM DTT, protease inhibitor, 0.5% Triton X-100, 15 mM Na_3VO_4, 10 mM p-nitrophenyl phosphate (alternatively 1 mM NaF was used), 1 μM okadaic acid). The beads preloaded with saturating amounts of GST or GST-14-3-3ε were incubated for 2 hours with lysed samples prepared from S2 cells or ovaries as described below. The beads were then washed 3 times in lysis buffer, and then twice in lysis buffer without detergent, and finally boiled in protein sample buffer.

To prepare S2 cell extract, S2 cells were cultured as described before (Dzhindzhev et al., 2005). For S2 cell RNAi depletion of Ncd, a mixture of dsRNAs targeting the 5' and 3' UTRs of Ncd were used, and 5 days of treatment resulted in the loss of the majority of Ncd protein. For S2 cell transfection, ~1.5 million cells in a final volume of 1.8 ml were plated in a well of a six well plate, and plasmids expressing Ncd-GFP under the metallothionein promoter in pMTWG were transfected using X-tremeGENE HP (Roche) following manufacturer's instructions. Copper sulphate was added to a final concentration of 0.7 mM. ~$5x10^7$ cells were pelleted at 500xg for 5 mins, resuspended in 500 μl of lysis buffer and left on ice for 30 min before being cleared by centrifugation at 13,000 rpm for 30 min at 4°C. To prepare ovary extract, ovaries were dissected at room temperature in PBS + 0.5% Triton X-100 and then transferred immediately to 1 ml of lysis buffer on ice. ~100 ovaries were ground with a glass dounce homogeniser and incubated on ice for 30 min before being cleared by centrifugation at 13,000 rpm for 30 min at 4°C.

In vitro kinase assay

An *in vitro* kinase assay using radiolabelled ATP was performed in 10 mM HEPES pH7.6, 50 mM KCl, 5 mM $MgCl_2$, 1% Triton X-100, 1 mM DTT, 1 mM PMSF and protease inhibitor (Fig. 3A). *E. coli* BL21(DE3) pLysS expressing wild-type or S96A mutant version of GST-Ncd(58-

192) were sonicated in the kinase buffer, spun down and 19 µl of the crude lysate was taken. 1 µl of human PKD2 (Millipore 14-506) diluted in kinase buffer to ~50 ng/µl or 1 µl of human CaMKIIα (BML-SE470) diluted in kinase buffer to ~50 ng/µl was added. ~5 µCi of ^{32}P-γ-ATP was added for 1 hour at room temperature, and the sample was boiled in protein sample buffer. The same approach was used for the non-radiolabelled *in vitro* phosphorylation, except that 200 µM of unlabelled ATP was used (Fig 3B). For western blots, proteins were transferred onto nitrocellulose membranes (Amersham Protran 0.2 NC, GE Healthcare Life Sciences) and generally stained for total protein using Reversible Protein Stain Kit for Nitrocellulose Membranes (Pierce).

Mass spectrometry

Protein samples were run on a gel (NuPAGE Novex 4-12% Bis-Tris gel, Life Technologies), in NuPAGE buffer (MES) and visualised using Imperial™ Protein Stain (Thermo Fisher Scientific). Gel lanes were cut excluding MBP/GST-14-3-3ε band, cut into smaller pieces, destained with ammonium bicarbonate and shrunk with acetonitrile before being reduced with dithiothreitol and alkylated with iodoacetamide. Buffer containing trypsin (Pierce) used for overnight digestion. Samples desalted with C18 stage tips (Rappsilber et al., 2007). Peptides were then analysed using a Velos LTQ Orbitrap (Thermo Scientific) coupled online to a Dionex RSLC nano system (Thermo Scientific). Samples were loaded directly onto a column needle self-packed with ReproSil-Pur C18-AQ material (3 µm; Dr Maisch, GmbH, Beim Bruckle, Germany) at a flow rate of 0.7 µl/min, using a spray emitter (75 µm ID, 8 µm opening, 300 mm length; new objective) and air-pressure pump (Proxeon, UK). For liquid chromatography a mobile phase A (MQ-H_2O, 0.1% formic acid) and mobile phase B (80% acetonitrile, 0.1% formic acid) were used. A 60-min gradient was used for the sample set, with a total run time of 100 min per sample. Raw data files were converted to .mgf file formats with MS Convert. Data analysis performed using Mascot using the following parameters: Mascot version: 2.4.1; enzyme: trypsin; maximum missed cleavages: 2; peptide tolerance: +/- 6ppm; MS/MS tolerance: +/- 0.6Da; for fixed modifications: carbamidomethylation on cysteine; for variable modifications: oxidation on

methionine. The database used was the combined UniProt *Drosophila melanogaster* database (September 2014). The mass spectrometry proteomics data have been deposited to the ProteomeXchange Consortium via the PRIDE partner repository (Vizcaíno, 2016)(http://www.ebi.ac.uk/pride) with the dataset identifier PXD006080 and 10.6019/PXD006080.

Protein purification

Glutathione S-transferase (GST)-tagged bacterial expression constructs for the tail region of Ncd (aa 58–192) were made in pGEX-6p-2. Maltose binding protein (MBP)-tagged bacterial expression constructs for 14-3-3ε were made in pMAL-C2. His-GFP tagged bacterial expression constructs for full length Ncd were made in pET-15b. For bacterial expression of proteins, bacteria were grown to OD_{600}=0.6 and shifted to 18°C prior to induction with 0.5 mM IPTG overnight. Bacteria were pelleted, washed in PBS and snap-frozen with liquid nitrogen. Pellets were resuspended in lysis buffer containing 50 mM Na-Phosphate buffer pH 7.6, 250 mM KCl, 1 mM $MgCl_2$, 5 mM β-mercaptoethanol and protease inhibitors (cOmplete™, Mini Protease Inhibitor Cocktail Tablets, Roche). Cells were lysed by sonication, and clarified by centrifugation 13,000 rpm for 30min at 4°C. Supernatant was incubated on a roller at 4°C with either washed glutathione-sepharose beads, or amylose beads for MBP-tagged proteins or with Talon resin for His-tagged proteins for 2 hours. Beads were subsequently washed 3 times in wash buffer (50 mM Na-Phosphate buffer pH 7.6, 250 mM KCl, 1mM $MgCl_2$, 5 mM β-mercaptoethanol, 50 mM Arginine and 50 mM glutamate). Washed beads were transferred to a column and elution of the protein of interest was done by sequential addition of elution buffer 50 mM Na-Phosphate buffer pH 7.6, 100 mM KCl, 1 mM $MgCl_2$, 5 mM β-mercaptoethanol, 50 mM arginine, 50 mM glutamate and 10 mM reduced glutathione for GST-tagged proteins, 5 mM maltose for MBP-tagged proteins and 200 mM imidazole for His-tagged proteins. Peak fractions judged by SDS-PAGE were combined and supplemented with 10% glycerol, snap-frozen in small aliquots and stored at −80°C for further use. His-tagged proteins were dialysed overnight in 50 mM Na-Phosphate buffer pH 7.6, 100mM KCl, 1 mM $MgCl_2$, 5 mM β-mercaptoethanol, 50 mM

arginine, 50 mM glutamate before addition of 10% glycerol, snap-frozen in small aliquots and stored at −80°C for further use.

Optimised phosphorylation conditions for Ncd tail

In vitro phosphorylation of purified wild-type Ncd or Ncd(S96A) tail was performed in 20 mM HEPES buffer pH=7.4, 2 mM $MgCl_2$, 1 mM ATP, 40 mM KCl, 1 mM DTT, 0.2 mg/ml BSA, 1 mM EGTA (Fig 3D, 4B-D, S2, S3). Human PKD2 (Millipore 14-506) to generate Ncd pS96 was diluted prior to use in kinase buffer (20 mM Tris pH=7.5, 50 mM NaCl and 0.1 mM EGTA) to a final concentration of 25 ng/µl. Human Aurora B (Millipore 14-835) to generate Ncd pS94 was diluted prior to use in kinase buffer 20 mM Tris pH=7.5, 50mM NaCl and 0.1mM EGTA to a final concentration of 100 ng/µl. Ncd substrate to kinase concentration ratio in the final kinase assay was 1/185 for PKD2 and 1/50 for Aurora B. Phosphorylation was carried out for 90 min at 30°C and kept on ice until required.

Microtubule pelleting assays

Taxol-stabilised microtubules were produced by incubating 60 µl of 5 mg/ml porcine tubulin, 6 µl of BRB80 cushion buffer with 40% glycerol, and 1.8 µl of 100 mM GTP at 37°C for 20 min. To stabilize the microtubules, 1.8 µl of 2 mM paclitaxel (taxol) in 110 µl of BRB80 was added to the microtubule polymerisation reaction. This tubulin stock mix (17 µM) was stored at room temperature until further use. Proteins to be tested were diluted in the same elution buffer in which they were purified or in the case of phosphorylation comparison assays in phosphorylation buffer to give the final concentrations defined in the figure legends. These protein mixes were then supplemented with BSA to a final concentration of 0.1 mg/ml, BRB80 containing taxol and microtubules were added to a final concentration of 3.5 µM. To ensure complete binding of 14-3-3 to Ncd, samples were incubated for 5 min prior to the addition of microtubules. Samples were incubated for 25 min at RT to bind microtubules and centrifuged for 13,000 rpm for 15 min. The supernatant was removed and mixed with 25 µl 3xSDS-PAGE sample buffer. The pellet was resuspended in 75 µl of 1xSDS-PAGE sample buffer. Equal amounts of both supernatant and pellet fractions were analysed by SDS-

PAGE and Western blotting. Phos-Tag gel (Wako-chem) was done according to manufacture using 25 µM Phos-tag and 50 µM $MnCl_2$.

MBP-14-3-3ε pulldown assay of purified Ncd

To test binding of control and phosphorylated versions of either Ncd or Ncd(S96A) to 14-3-3ε, Ncd or Ncd(S96A) were phosphorylated using PKD2 or Aurora B to generate pS94 or pS96 or both. A final amount of 3.75 µg of Ncd tail was added with 10 µg of MBP-14-3-3ε and diluted in pull down buffer to a final volume of 500 µl with 25 mM Tris-Cl pH=7.6, 150 mM NaCl, 0.5% Triton X-100, 0.3 mM $NaVO_4$, 0.1 mg/ml BSA and incubated on ice for 30 min. 20 µl of Amylose resin pre-washed and equilibrated in pull-down buffer was added and incubated for 1 hour on roller at 4°C. Resin was washed two times with pull down buffer and 30 µl of 1.5xSDS-PAGE sample buffer was added and analysed by either normal SDS-PAGE or 25 µM Phos-tag and 50 µM $MnCl_2$ for Western blotting.

List of supplementary data

Figure S1. Effects of 14-3-3 and Ncd on the meiotic spindle in oocytes

Figure S2. Ncd microtubule binding affinity is not affected by changes in the charge of S96

Figure S3. 14-3-3 inhibits Ncd microtubule binding, by binding to phosphorylated S96

Table S1. Mass spectrometry data from 14-3-3ε pulldown

Acknowledgements

We are grateful to C. MacKintosh for her advice, to all the members of the Ohkura lab and D. Finnegan for their help and useful feedback, to E. Peat, C. Barnard and D. Staneva for their contributions, to Y. Matsubayashi for his ImageJ plug-in, to D. Kelly for his help, and to the Bloomington Drosophila Stock Center and Resource Center (NIH P40OD018537, 2P40OD010949-10A1) and the Transgenic RNAi Project at Harvard Medical School

(NIH/NIGMS R01-GM084947) for fly stocks. Wellcome Trust Senior Research Fellowships (103139, 098030) to JR and HO. The Wellcome Centre for Cell Biology is supported by a core grant (077707, 092076, 203149) and the work was also supported by Wellcome Trust instrument grant 108504.

The authors declare no competing financial interests.

Author contributions: RB, RNB, CS, PR, CFC designed and performed experiments, and wrote manuscript; JR, RG, GG, HO designed experiments and wrote the manuscript.

References

Ashburner, M., and C.M. Bergman. 2005. Drosophila melanogaster: a case study of a model genomic sequence and its consequences. *Genome Res*. 15:1661-1667.

Benton, R., I.M. Palacios, and D. St Johnston. 2002. Drosophila 14-3-3/PAR-5 is an essential mediator of PAR-1 function in axis formation. *Dev Cell*. 3:659-671.

Benton, R., and D. St Johnston. 2003. Drosophila PAR-1 and 14-3-3 inhibit Bazooka/PAR-3 to establish complementary cortical domains in polarized cells. *Cell*. 115:691-704.

Bodenmiller, B., J. Malmstrom, B. Gerrits, D. Campbell, H. Lam, A. Schmidt, O. Rinner, L.N. Mueller, P.T. Shannon, P.G. Pedrioli, C. Panse, H.K. Lee, R. Schlapbach, and R. Aebersold. 2007. PhosphoPep--a phosphoproteome resource for systems biology research in Drosophila Kc167 cells. *Mol Syst Biol*. 3:139.

Carazo-Salas, R.E., G. Guarguaglini, O.J. Gruss, A. Segref, E. Karsenti, and I.W. Mattaj. 1999. Generation of GTP-bound Ran by RCC1 is required for chromatin-induced mitotic spindle formation. *Nature*. 400:178-181.

Cesario, J., and K.S. McKim. 2011. RanGTP is required for meiotic spindle organization and the initiation of embryonic development in Drosophila. *J Cell Sci*. 124:3797-3810.

Chang, H.C., and G.M. Rubin. 1997. 14-3-3 epsilon positively regulates Ras-mediated signaling in Drosophila. *Genes Dev*. 11:1132-1139.

Colombié, N., C.F. Cullen, A.L. Brittle, J.K. Jang, W.C. Earnshaw, M. Carmena, K. McKim, and H. Ohkura. 2008. Dual roles of Incenp crucial to the assembly of the acentrosomal metaphase spindle in female meiosis. *Development*. 135:3239-3246.

Cullen, C.F., and H. Ohkura. 2001. Msps protein is localized to acentrosomal poles to ensure bipolarity of Drosophila meiotic spindles. *Nat Cell Biol*. 3:637-642.

Darling, D.L., J. Yingling, and A. Wynshaw-Boris. 2005. Role of 14-3-3 proteins in eukaryotic signaling and development. *Curr Top Dev Biol*. 68:281-315.

De, S., and D. Kline. 2013. Evidence for the requirement of 14-3-3eta (YWHAH) in meiotic spindle assembly during mouse oocyte maturation. *BMC Dev Biol*. 13:10.

Douglas, M.E., T. Davies, N. Joseph, and M. Mishima. 2010. Aurora B and 14-3-3 coordinately regulate clustering of centralspindlin during cytokinesis. *Curr Biol*. 20:927-933.

Dumont, J., S. Petri, F. Pellegrin, M.E. Terret, M.T. Bohnsack, P. Rassinier, V. Georget, P. Kalab, O.J. Gruss, and M.H. Verlhac. 2007. A centriole- and RanGTP-independent spindle assembly pathway in meiosis I of vertebrate oocytes. *J Cell Biol*. 176:295-305.

Dzhindzhev, N.S., S.L. Rogers, R.D. Vale, and H. Ohkura. 2005. Distinct mechanisms govern the localisation of Drosophila CLIP-190 to unattached kinetochores and microtubule plus-ends. *J Cell Sci*. 118:3781-3790.

Endow, S.A., and D.J. Komma. 1997. Spindle dynamics during meiosis in Drosophila oocytes. *J Cell Biol*. 137:1321-1336.

Gardino, A.K., and M.B. Yaffe. 2011. 14-3-3 proteins as signaling integration points for cell cycle control and apoptosis. *Semin Cell Dev Biol*. 22:688-695.

Giet, R., D. McLean, S. Descamps, M.J. Lee, J.W. Raff, C. Prigent, and D.M. Glover. 2002. Drosophila Aurora A kinase is required to localize D-TACC to centrosomes and to regulate astral microtubules. *J Cell Biol*. 156:437-451.

Gluszek, A.A., C.F. Cullen, W. Li, R.A. Battaglia, S.J. Radford, M.F. Costa, K.S. McKim, G. Goshima, and H. Ohkura. 2015. The microtubule catastrophe promoter Sentin delays stable kinetochore-microtubule attachment in oocytes. *J Cell Biol*. 211:1113-1120.

Goshima, G., R. Wollman, S.S. Goodwin, N. Zhang, J.M. Scholey, R.D. Vale, and N. Stuurman. 2007. Genes required for mitotic spindle assembly in Drosophila S2 cells. *Science*. 316:417-421.

Gruss, O.J., R.E. Carazo-Salas, C.A. Schatz, G. Guarguaglini, J. Kast, M. Wilm, N. Le Bot, I. Vernos, E. Karsenti, and I.W. Mattaj. 2001. Ran induces spindle assembly by reversing the inhibitory effect of importin alpha on TPX2 activity. *Cell*. 104:83-93.

Hatsumi, M., and S.A. Endow. 1992. Mutants of the microtubule motor protein, nonclaret disjunctional, affect spindle structure and chromosome movement in meiosis and mitosis. *J Cell Sci*. 101 (Pt 3):547-559.

Hilger, M., T. Bonaldi, F. Gnad, and M. Mann. 2009. Systems-wide analysis of a

phosphatase knock-down by quantitative proteomics and phosphoproteomics. *Mol Cell Proteomics*. 8:1908-1920.

Johnson, C., S. Crowther, M.J. Stafford, D.G. Campbell, R. Toth, and C. MacKintosh. 2010. Bioinformatic and experimental survey of 14-3-3-binding sites. *Biochem J.* 427:69-78.

Kalab, P., R.T. Pu, and M. Dasso. 1999. The ran GTPase regulates mitotic spindle assembly. *Curr Biol*. 9:481-484.

Karabay, A., and R.A. Walker. 1999. Identification of microtubule binding sites in the Ncd tail domain. *Biochemistry*. 38:1838-1849.

Kimble, M., and K. Church. 1983. Meiosis and early cleavage in Drosophila melanogaster eggs: effects of the claret-non-disjunctional mutation. *J Cell Sci*. 62:301-318.

Kockel, L., G. Vorbruggen, H. Jackle, M. Mlodzik, and D. Bohmann. 1997. Requirement for Drosophila 14-3-3 zeta in Raf-dependent photoreceptor development. *Genes Dev*. 11:1140-1147.

Loh, B.J., C.F. Cullen, N. Vogt, and H. Ohkura. 2012. The conserved kinase SRPK regulates karyosome formation and spindle microtubule assembly in Drosophila oocytes. *J Cell Sci*. 125:4457-4462.

Matthies, H.J., H.B. McDonald, L.S. Goldstein, and W.E. Theurkauf. 1996. Anastral meiotic spindle morphogenesis: role of the non-claret disjunctional kinesin-like protein. *J Cell Biol*. 134:455-464.

Morrison, D.K. 2009. The 14-3-3 proteins: integrators of diverse signaling cues that impact cell fate and cancer development. *Trends Cell Biol*. 19:16-23.

Moutinho-Pereira, S., N. Stuurman, O. Afonso, M. Hornsveld, P. Aguiar, G. Goshima, R.D. Vale, and H. Maiato. 2013. Genes involved in centrosome-independent mitotic spindle assembly in Drosophila S2 cells. *Proc Natl Acad Sci U S A*. 110:19808-19813.

Nachury, M.V., T.J. Maresca, W.C. Salmon, C.M. Waterman-Storer, R. Heald, and K. Weis. 2001. Importin beta is a mitotic target of the small GTPase Ran in spindle assembly. *Cell*. 104:95-106.

Ohba, T., M. Nakamura, H. Nishitani, and T. Nishimoto. 1999. Self-organization of microtubule asters induced in Xenopus egg extracts by GTP-bound Ran. *Science*.

284:1356-1358.

Ohkura, H. (2015) Meiosis: An overview of key differences from mitosis. Cold Spring Harb Perspect Biol. 7: a015859.

Ohi, R., T. Sapra, J. Howard, and T.J. Mitchison. 2004. Differentiation of cytoplasmic and meiotic spindle assembly MCAK functions by Aurora B-dependent phosphorylation. *Mol Biol Cell*. 15:2895-2906.

Pearson, N.J., C.F. Cullen, N.S. Dzhindzhev, and H. Ohkura. 2005. A pre-anaphase role for a Cks/Suc1 in acentrosomal spindle formation of Drosophila female meiosis. *EMBO Rep*. 6:1058-1063.

Radford, S.J., A.M. Harrison, and K.S. McKim. 2012a. Microtubule-depolymerizing kinesin KLP10A restricts the length of the acentrosomal meiotic spindle in Drosophila females. *Genetics*. 192:431-440.

Radford, S.J., J.K. Jang, and K.S. McKim. 2012b. The chromosomal passenger complex is required for meiotic acentrosomal spindle assembly and chromosome biorientation. *Genetics*. 192:417-429.

Rappsilber, J., M. Mann, and Y. Ishihama. 2007. Protocol for micro-purification, enrichment, pre-fractionation and storage of peptides for proteomics using StageTips. *Nat Protoc*. 2:1896-1906.

Sampath, S.C., R. Ohi, O. Leismann, A. Salic, A. Pozniakovski, and H. Funabiki. 2004. The chromosomal passenger complex is required for chromatin-induced microtubule stabilization and spindle assembly. *Cell*. 118:187-202.

Skold, H.N., D.J. Komma, and S.A. Endow. 2005. Assembly pathway of the anastral Drosophila oocyte meiosis I spindle. *J Cell Sci*. 118:1745-1755.

Sumiyoshi, E., Y. Fukata, S. Namai, and A. Sugimoto. 2015. Caenorhabditis elegans Aurora A kinase is required for the formation of spindle microtubules in female meiosis. *Mol Biol Cell*. 26:4187-4196.

Swain, J.E., J. Ding, J. Wu, and G.D. Smith. 2008. Regulation of spindle and chromatin dynamics during early and late stages of oocyte maturation by aurora kinases. *Mol Hum Reprod*. 14:291-299.

Tseng, B.S., L. Tan, T.M. Kapoor, and H. Funabiki. 2010. Dual detection of chromosomes and microtubules by the chromosomal passenger complex drives spindle assembly. *Dev Cell*. 18:903-912.

Wiese, C., A. Wilde, M.S. Moore, S.A. Adam, A. Merdes, and Y. Zheng. 2001. Role of importin-beta in coupling Ran to downstream targets in microtubule assembly. *Science*. 291:653-656.

Wilde, A., and Y. Zheng. 1999. Stimulation of microtubule aster formation and spindle assembly by the small GTPase Ran. *Science*. 284:1359-1362.

Zhai, B., J. Villen, S.A. Beausoleil, J. Mintseris, and S.P. Gygi. 2008. Phosphoproteome analysis of Drosophila melanogaster embryos. *J Proteome Res*. 7:1675-1682.

Figure Legends

Figure 1. Loss of 14-3-3 results in disrupted organisation of female meiotic spindles and Msps pole localisation

(A-C) Meiotic spindle morphologies in immunostained mature metaphase-I arrested oocytes depleted of 14-3-3. ***p<0.001, *p=0.013. (A) n=170,174,16,17. (B) n=17,17,21,18. (C) n=49,65. Error bars represent 95% confidence intervals. (D) Live imaging of mature oocytes expressing GFP-α-tubulin. Bars=10 μm.

Figure 2. 14-3-3 binding to Ncd is important for Ncd association with meiotic spindles and spindle bipolarity in oocytes

(A) Western blot of ovary extract and pull-down fractions with GST-14-3-3ε or GST control, probed by an anti-Ncd antibody. (B) Ncd with the main 14-3-3 binding site (S96), and strong (dark green) and weaker (pale green) microtubule binding regions indicated. (C) Western blot, probed by a GFP antibody, and protein staining of pull-down fractions with GST-14-3-3ε from lysates of S2 cells expressing wild-type, S96A or 3xA versions of Ncd-GFP, but depleted of the endogenous Ncd. (D) Immunostaining of spindles in *ncd*^{1} mutant oocytes carrying no transgenes, one Ncd-GFP transgene or two Ncd(S96A)-GFP transgenes. GFP signals were captured and modified using identical settings. Bar=10 μm. (E) GFP signal intensity relative to α-tubulin signal on the spindle. n=10,22. **p<0.01. This experiment was repeated using a different microscopy in Fig 5B. (F) Spindle morphologies in oocytes. n=170,45,10,50. ***p<0.001.

Figure 3. 14-3-3 inhibits Ncd microtubule binding

(A) Kinase assay using PKD2 or CAMKIIα, Ncd(58-192) with or without the S96A mutation, and ^{32}P-ATP. (B) Western blot, probed by a phospho-S96 Ncd antibody, and total protein staining of fractions pulled down by MBP-14-3-3ε after kinase assay with cold ATP. (C) Microtubule binding assay. Ncd or Ncd(S96A) was incubated with PKD2 and/or Aurora B or

without, and mixed with microtubules and GST-14-3-3ε before spinning down. (D) Microtubule binding assay of the Ncd tails with or without MBP-14-3-3ε.

Figure 4. Aurora B releases Ncd from inhibition by 14-3-3

(A) Western blot, probed by an anti-GFP antibody, of pulldown with GST-14-3-3ε from extracts of S2 cells transiently expressing various versions of Ncd-GFP but depleted of the endogenous Ncd. (B) Kinase assay. Coomassie-stained PhosTag gel of the Ncd(58-192) and BSA incubated with kinases. (C) GFP-tagged Ncd tail phosphorylated by kinases (input) and pulled-down fraction with MBP-14-3-3ε. (D) Microtubule binding assay of differently phosphorylated Ncd tails with or without MBP-14-3-3ε.

Figure 5. Aurora B phosphorylation is important for targeting Ncd to the spindle and spindle bipolarity

(A) Immunostaining of spindles in *ncd*^{1} mutant oocytes carrying one Ncd-GFP transgene or one Ncd(S94A)-GFP transgene. Images were captured and modified using an identical setting. Bar=10 μm. (B) GFP signal intensity relative to α-tubulin signal on the spindle. n=34,27,41. ***p<0.001. **p<0.01. Note that these were imaged using a different microscope to Figure 2. (C) Spindle morphologies in oocytes. n=31,42. (D,E) Aurora B releases Ncd from 14-3-3 inhibition in oocytes, analogously to the Ran-importin system, enabling Ncd to specifically bind spindle MTs.

Supplementary Data

Figure S1. Effects on 14-3-3 and Ncd on the meiotic spindle in oocytes

(A) Quantification of spindle morphology in different conditions, including data shown in Fig. 1A, 2F, 5C. n=59,19,135,39,44,33,16,17,32,23,22,13,10,50,22,31,42. (B) Western blot probed with an anti-GFP antibody and total protein staining of ovary samples. One copy of Ncd-GFP, one copy of Ncd(94A)-GFP and two copies of Ncd(96A)-GFP produced comparable level of Ncd-GFP variants. (C) Immunostained metaphase I arrested spindles from control and 14-3-3ε RNAi (using a stronger driver MDD). Images were taken and modified with identical settings. Bar=10μm. (D) Western blots of ovary samples, and quantification of Ncd or 14-3-3ε signal intensity normalised by tubulin intensity. (E) Ncd signal intensity relative to α-tubulin signal with values normalised to the median control value of each experiment. Strong (MDD) and weak (V2H) drivers were used as well as the routinely used driver (V37). Plots indicate lower quartile, median and upper quartile. n=159,37,117,14. ***p<0.001, *p<0.05. (F) Distribution of Ncd and α-tubulin signal intensities along spindles (from pole to pole) in oocytes depleted of 14-3-3ε (using the strong driver MDD). Error bars represent SEMs. n=17, 21.

Figure S2. Ncd microtubule binding affinity is not affected by alanine mutation or phosphorylation at S96

(A) 14-3-3ε docking to phosphorylated S96 reduced the affinity of Ncd tail to microtubules. Wild-type (wt) Ncd tail was first incubated with PKD2 to generate phosphorylation on S96, or without PKD2 as control. Then it was incubated with different concentrations of microtubules and MBP-14-3-3ε (or without MBP-14-3-3ε as control) before spinning down. Pellet and supernatant samples were run on standard SDS gels, which were stained with Coomassie or subjected to western blotting using the phospho-S96 specific Ncd antibody. The percentage of Ncd tail found in the microtubule pellet is displayed at the bottom of each lane. Intensity

of Coomassie-stained Ncd tail in the pellet fractions in either wt Ncd or phosphorylated Ncd (at S96) in the presence (upper) or absence (lower) of 14-3-3ε is displayed in the middle panels. The amount of Ncd tail bound to microtubules as a function of the amount of Ncd tail added is displayed in the right panel. Error bars represent SDs (n=3). (B) Wt Ncd and Ncd(S96A) tail have the same affinity to microtubules. Variable concentrations of wt Ncd or Ncd (S96A) tail were incubated with microtubules and spun down. The percentage of Ncd tail found in the microtubule pellet is indicated at the bottom of each lane. Quantification of the amount of Ncd tail found in the pellets and supernatant for either wt Ncd or Ncd(S96A) tail is displayed in the middle panels. The right panel displays the amount of Ncd tail bound to microtubules as a function of the amount of Ncd tail added in a representative experiment (n=4). (C-E) Quantification and controls related to Fig. 3D. Quantification of the Coomassie-stained standard SDS gel shows the amount of tubulin (C) or Ncd tail (D) found in the pellet and supernatant. Error bars represent SDs (n=3). (E) wt Ncd and Ncd(S96A) incubated with or without PKD2 in the absence of microtubules are detected in the supernatant in the microtubule binding assay.

Figure S3. 14-3-3 inhibits Ncd microtubule binding by docking to phosphorylated S96

(A) Ncd(S96A) binding to microtubules was not disrupted by incubation with PKD2 or Aurora B or by the presence of 14-3-3ε. Ncd(S96A) was incubated first with no kinases, PKD2 alone, Aurora B alone or PKD2 and Aurora B, and then with MBP-14-3-3ε prior to the addition of microtubules before spinning down. Coomassie-stained standard SDS gel of pellet and supernatant samples, and PhosTag gel followed by western blots using the Ncd antibody showing the absence of motility shift when treated with PKD2. The percentages of Ncd tail found in the microtubule pellet are indicated at the bottom of each lane. (B) Quantification of the amount of Ncd tail found in the pellets and supernatant for either wt Ncd (upper panel, related to Fig. 4D) or Ncd(S96A) tail (lower panel, related to Fig. S3A). Error bars represent SDs (n=3). (C) Binding control related to Fig. 4D, wt Ncd incubated with no

kinases, PKD2 alone, Aurora B alone or both was found in the supernatant when microtubules were omitted from the microtubule binding assay.

Table S1. Mass spectrometry data from 14-3-3ε pulldown

Mass spectrometry peptide hits from MBP or GST-14-3-3ε pulldown experiments from ovary or S2 cell extract, as indicated.

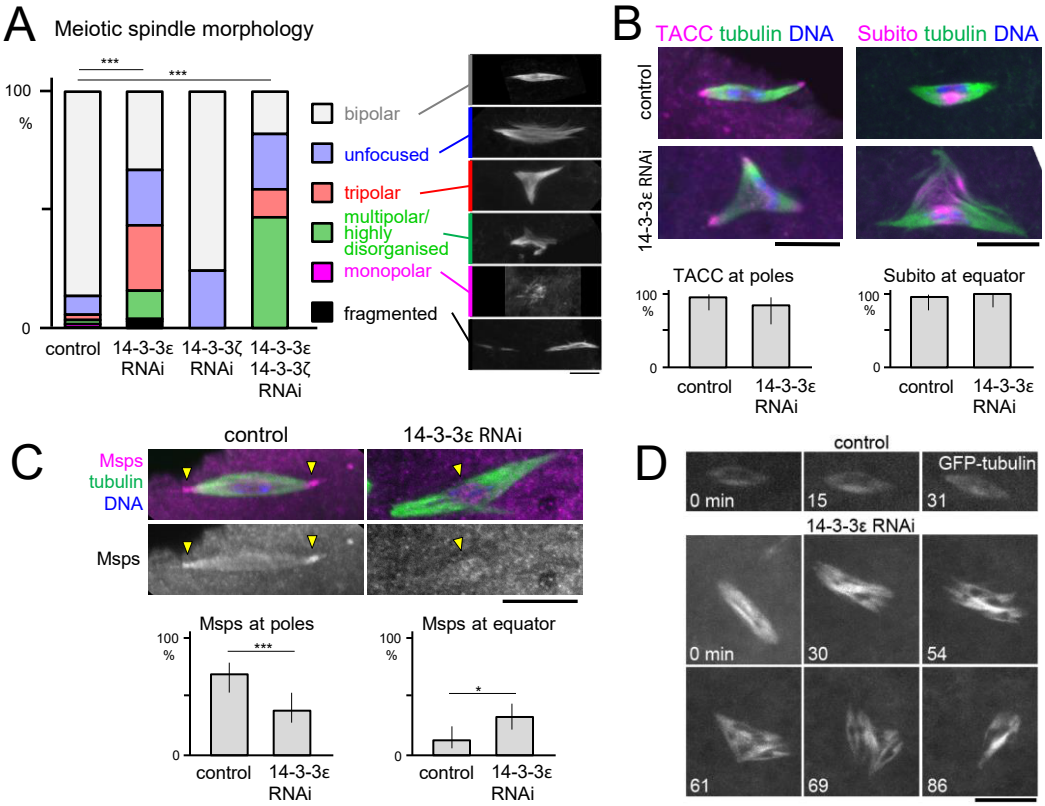
A
Meiotic spindle morphology
***
***
100
%
0
control
14-3-3ε RNAi
14-3-3ζ RNAi
14-3-3ε 14-3-3ζ RNAi
bipolar
unfocused
tripolar
multipolar/ highly disorganised
monopolar
fragmented
B
TACC tubulin DNA
Subito tubulin DNA
control
14-3-3ε RNAi
TACC at poles
Subito at equator
100
%
0
control
14-3-3ε RNAi
C
control
14-3-3ε RNAi
Msps tubulin DNA
Msps
Msps at poles
Msps at equator
***
*
100
%
0
control
14-3-3ε RNAi
D
control
GFP-tubulin
0 min
15
31
14-3-3ε RNAi
0 min
30
54
61
69
86

Figure 1

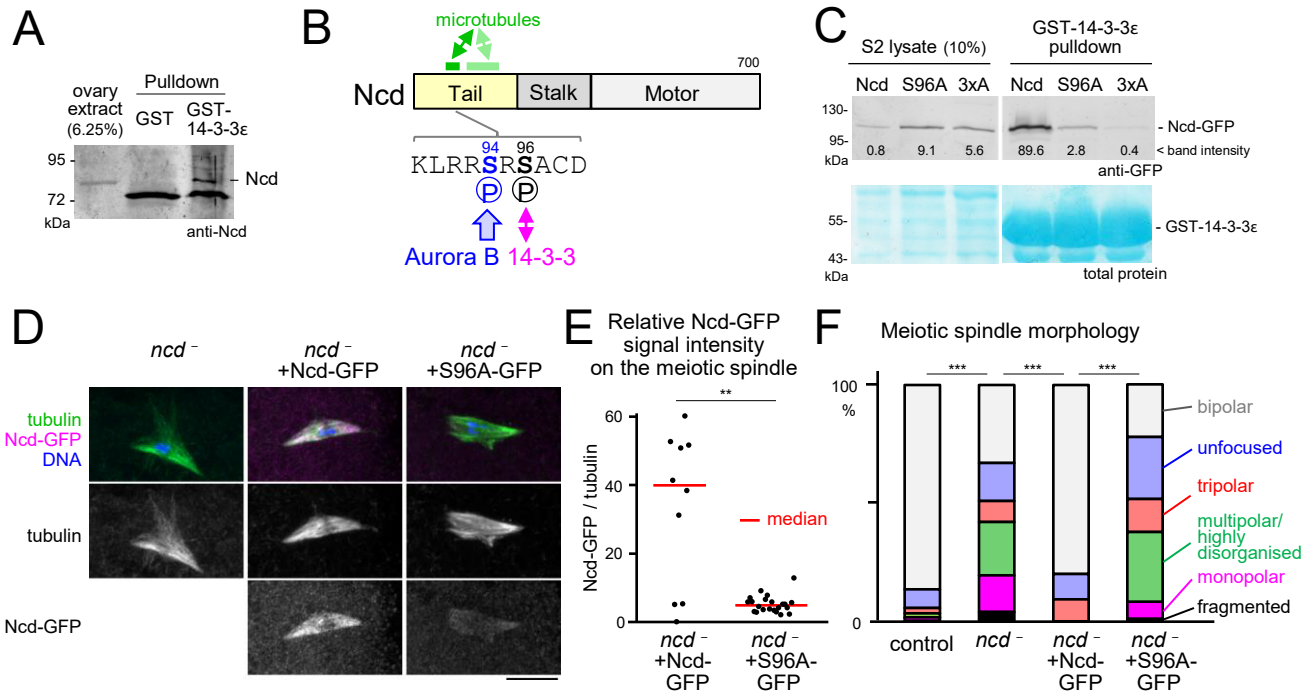
A
ovary extract (6.25%)
Pulldown
GST
GST-14-3-3ε
95
72
kDa
Ncd
anti-Ncd
B
microtubules
Ncd
Tail
Stalk
Motor
700
94
96
KLRRSRSACD
Aurora B
14-3-3
C
S2 lysate (10%)
GST-14-3-3ε pulldown
Ncd
S96A
3xA
130-
95-
kDa
0.8
9.1
5.6
89.6
2.8
0.4
- Ncd-GFP
< band intensity
anti-GFP
55-
43-
- GST-14-3-3ε
total protein
D
ncd⁻
ncd⁻ +Ncd-GFP
ncd⁻ +S96A-GFP
tubulin
Ncd-GFP
DNA
tubulin
Ncd-GFP
E
Relative Ncd-GFP signal intensity on the meiotic spindle
**
Ncd-GFP / tubulin
60
40
20
0
median
ncd⁻ +Ncd-GFP
ncd⁻ +S96A-GFP
F
Meiotic spindle morphology
***
***
***
100 %
0
bipolar
unfocused
tripolar
multipolar/ highly disorganised
monopolar
fragmented
control
ncd⁻
ncd⁻ +Ncd-GFP
ncd⁻ +S96A-GFP

Figure 2

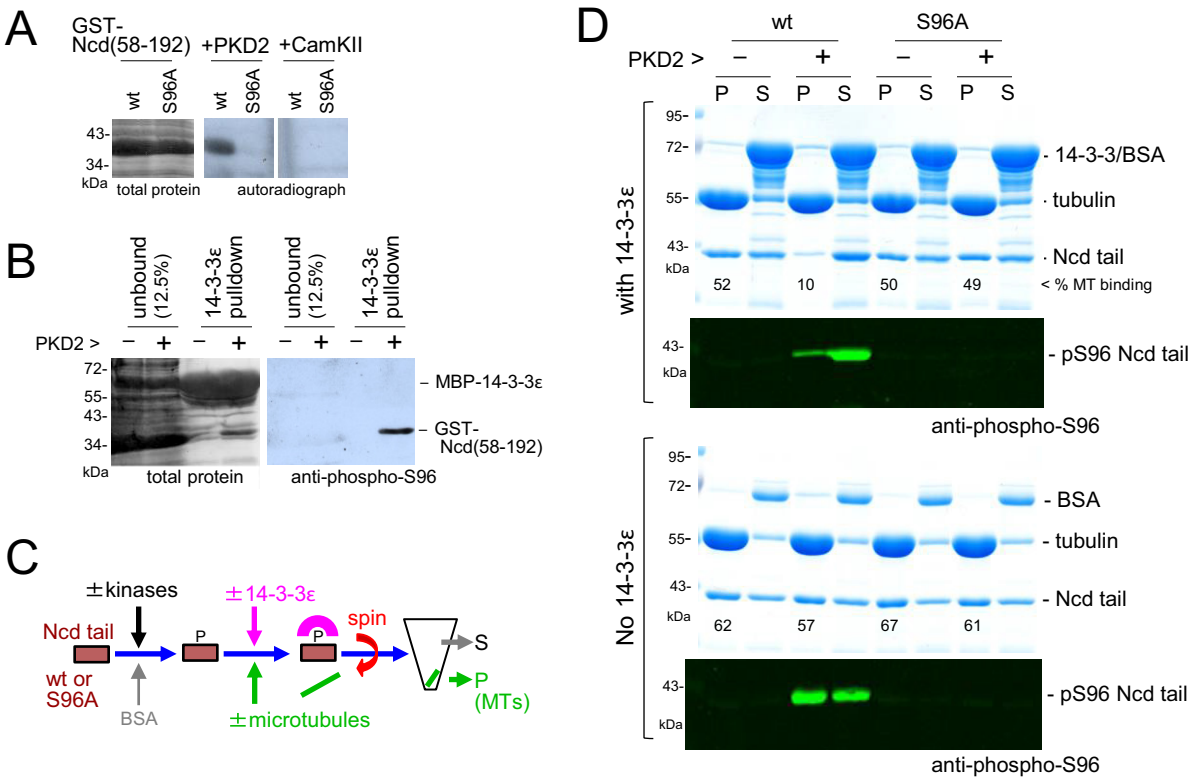
A
GST-
Ncd(58-192)
+PKD2
+CamKII
wt
S96A
wt
S96A
wt
S96A
43-
34-
kDa
total protein
autoradiograph
B
unbound
(12.5%)
14-3-3ε
pulldown
unbound
(12.5%)
14-3-3ε
pulldown
PKD2 >
– + – + – + – +
72-
55-
43-
34-
kDa
– MBP-14-3-3ε
– GST-
Ncd(58-192)
total protein
anti-phospho-S96
C
±kinases
Ncd tail
wt or
S96A
BSA
P
±14-3-3ε
P
spin
S
P
(MTs)
±microtubules
D
wt
S96A
PKD2 >
– + – +
P S P S P S P S
with 14-3-3ε
95-
72-
55-
43-
kDa
- 14-3-3/BSA
· tubulin
· Ncd tail
52
10
50
49
< % MT binding
43-
kDa
- pS96 Ncd tail
anti-phospho-S96
No 14-3-3ε
95-
72-
55-
43-
kDa
- BSA
- tubulin
- Ncd tail
62
57
67
61
43-
kDa
- pS96 Ncd tail
anti-phospho-S96

Figure 3

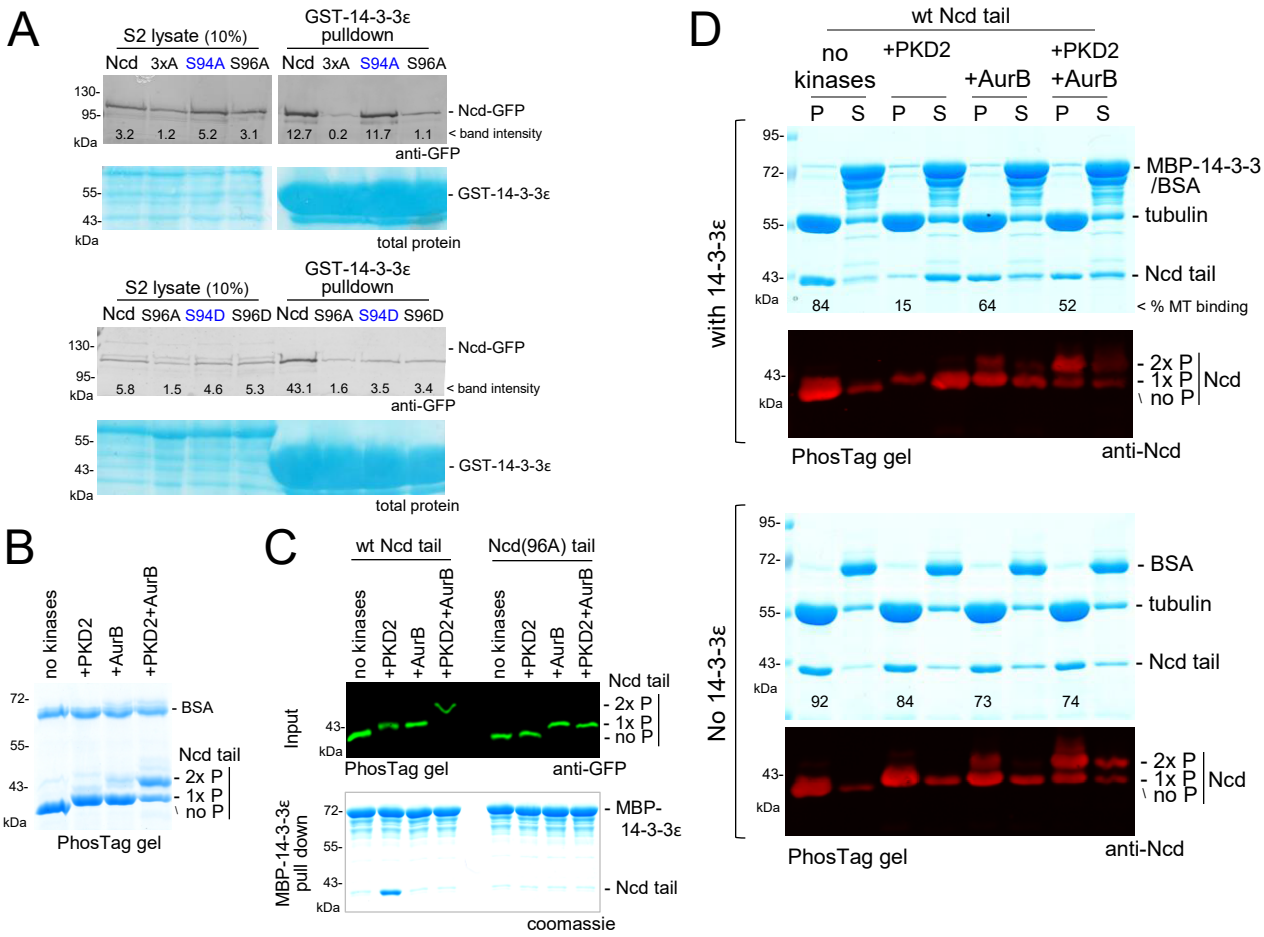
A
S2 lysate (10%)
GST-14-3-3ε pulldown
Ncd 3xA S94A S96A Ncd 3xA S94A S96A
130-
95-
kDa
3.2 1.2 5.2 3.1
12.7 0.2 11.7 1.1
- Ncd-GFP
< band intensity
anti-GFP
55-
43-
kDa
- GST-14-3-3ε
total protein
S2 lysate (10%)
GST-14-3-3ε pulldown
Ncd S96A S94D S96D Ncd S96A S94D S96D
5.8 1.5 4.6 5.3 43.1 1.6 3.5 3.4
- Ncd-GFP
< band intensity
anti-GFP
- GST-14-3-3ε
total protein
B
no kinases
+PKD2
+AurB
+PKD2+AurB
72-
55-
43-
kDa
- BSA
Ncd tail
- 2x P
- 1x P
\ no P
PhosTag gel
C
wt Ncd tail
Ncd(96A) tail
no kinases
+PKD2
+AurB
+PKD2+AurB
Input
43-
kDa
Ncd tail
- 2x P
- 1x P
- no P
PhosTag gel
anti-GFP
MBP-14-3-3ε pull down
72-
55-
43-
kDa
- MBP-14-3-3ε
- Ncd tail
coomassie
D
wt Ncd tail
no kinases
+PKD2
+AurB
+PKD2 +AurB
P S P S P S P S
with 14-3-3ε
95-
72-
55-
43-
kDa
- MBP-14-3-3 /BSA
- tubulin
- Ncd tail
84 15 64 52
< % MT binding
- 2x P
- 1x P
- no P
Ncd
PhosTag gel
anti-Ncd
No 14-3-3ε
- BSA
- tubulin
- Ncd tail
92 84 73 74
- 2x P
- 1x P
- no P
Ncd
PhosTag gel
anti-Ncd

Figure 4

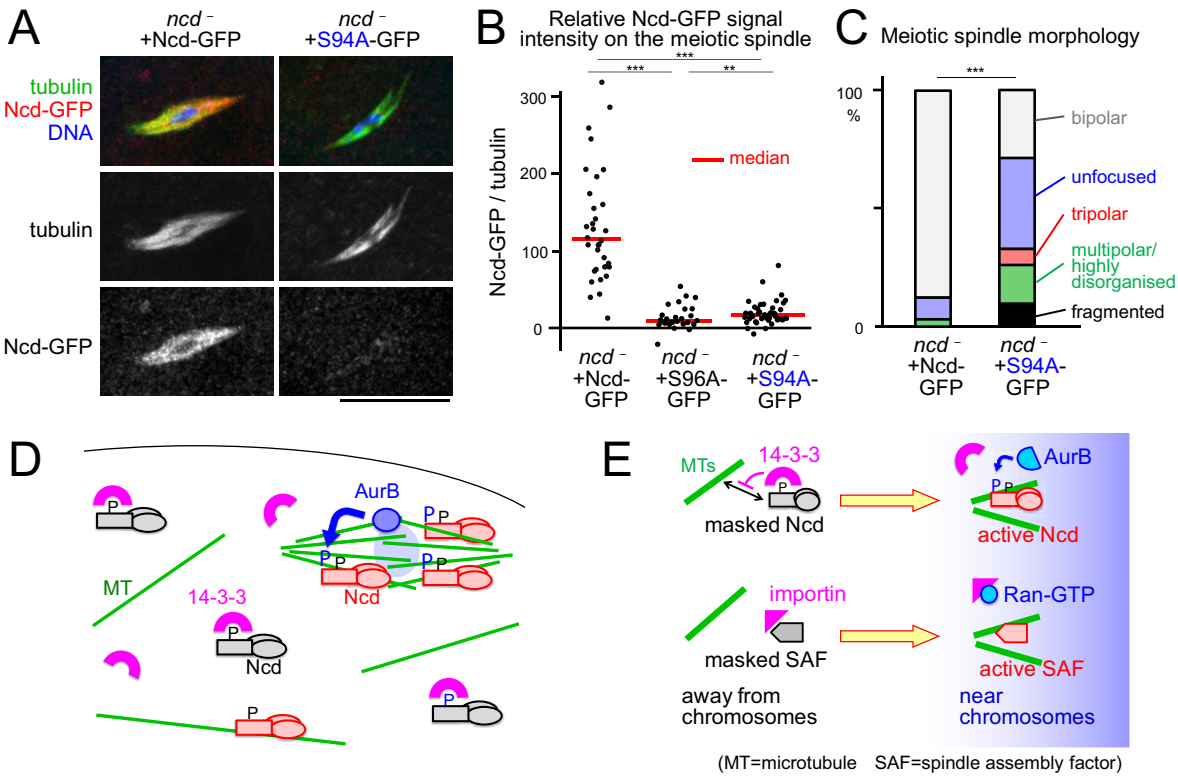
A
ncd⁻ +Ncd-GFP
ncd⁻ +S94A-GFP
tubulin
Ncd-GFP
DNA
tubulin
Ncd-GFP
B
Relative Ncd-GFP signal intensity on the meiotic spindle
Ncd-GFP / tubulin
300
200
100
0
median
***
***
**
ncd⁻ +Ncd-GFP
ncd⁻ +S96A-GFP
ncd⁻ +S94A-GFP
C
Meiotic spindle morphology
100 %
0
***
bipolar
unfocused
tripolar
multipolar/ highly disorganised
fragmented
ncd⁻ +Ncd-GFP
ncd⁻ +S94A-GFP
D
AurB
P
MT
14-3-3
Ncd
E
MTs
14-3-3
masked Ncd
active Ncd
AurB
importin
masked SAF
away from chromosomes
Ran-GTP
active SAF
near chromosomes
(MT=microtubule SAF=spindle assembly factor)

Figure 5

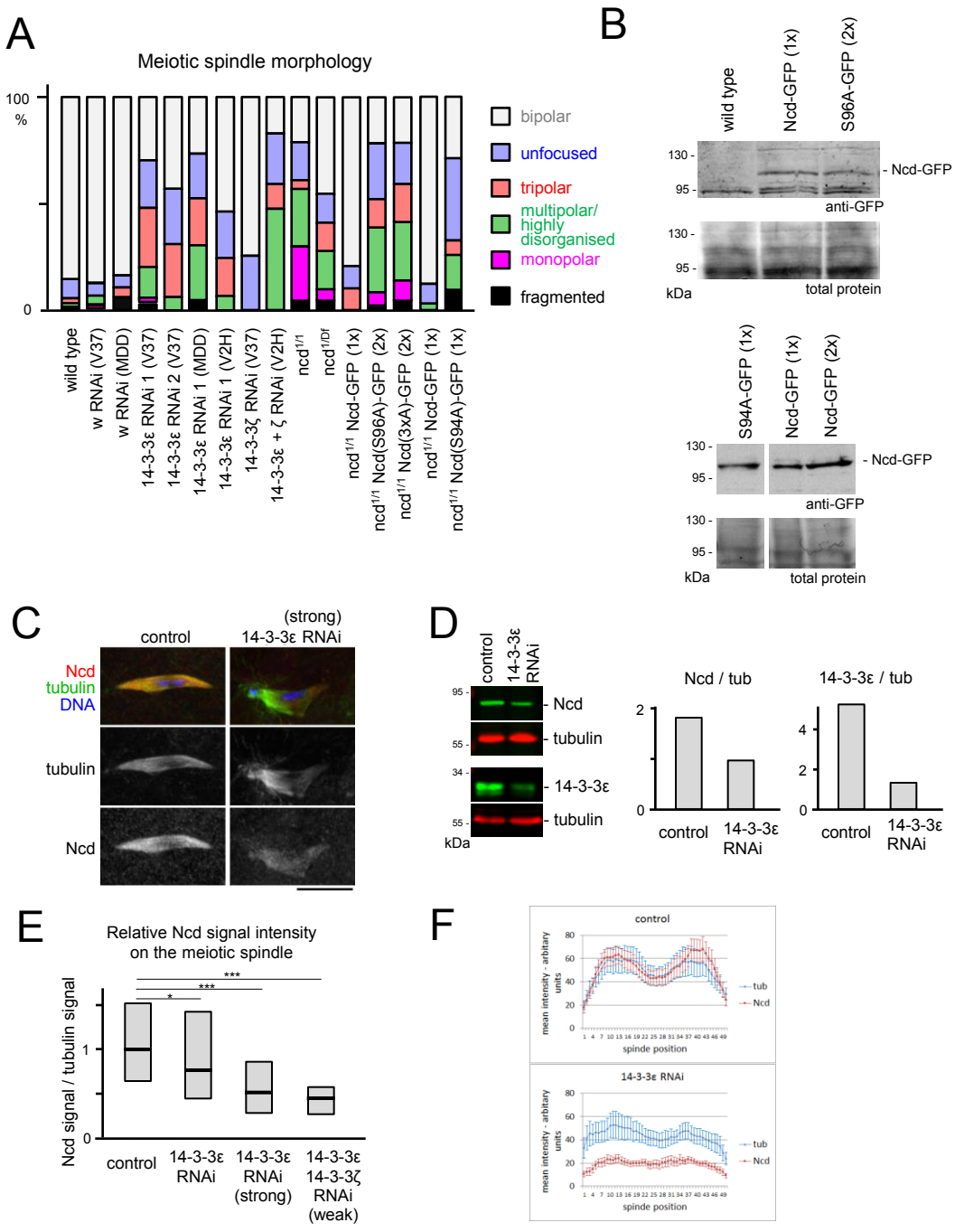
A
Meiotic spindle morphology
100 %
0
bipolar
unfocused
tripolar
multipolar/ highly disorganised
monopolar
fragmented
wild type
w RNAi (V37)
w RNAi (MDD)
14-3-3ε RNAi 1 (V37)
14-3-3ε RNAi 2 (V37)
14-3-3ε RNAi 1 (MDD)
14-3-3ε RNAi 1 (V2H)
14-3-3ζ RNAi (V37)
14-3-3ε + ζ RNAi (V2H)
ncd1/1
ncd1/Df
ncd1/1 Ncd-GFP (1x)
ncd1/1 Ncd(S96A)-GFP (2x)
ncd1/1 Ncd(3xA)-GFP (2x)
ncd1/1 Ncd-GFP (1x)
ncd1/1 Ncd(S94A)-GFP (1x)
B
wild type
Ncd-GFP (1x)
S96A-GFP (2x)
130 -
95 -
- Ncd-GFP
anti-GFP
130 -
95 -
kDa
total protein
S94A-GFP (1x)
Ncd-GFP (1x)
Ncd-GFP (2x)
130 -
95 -
- Ncd-GFP
anti-GFP
130 -
95 -
kDa
total protein
C
control
(strong) 14-3-3ε RNAi
Ncd
tubulin
DNA
tubulin
Ncd
D
control
14-3-3ε RNAi
95 -
Ncd
55 -
tubulin
34 -
14-3-3ε
55 -
tubulin
kDa
Ncd / tub
2
0
control
14-3-3ε RNAi
14-3-3ε / tub
4
2
0
control
14-3-3ε RNAi
E
Relative Ncd signal intensity on the meiotic spindle
***
***
*
Ncd signal / tubulin signal
1
0
control
14-3-3ε RNAi
14-3-3ε RNAi (strong)
14-3-3ε 14-3-3ζ RNAi (weak)
F
control
mean intensity - arbitary units
spinde position
tub
Ncd
14-3-3ε RNAi
mean intensity - arbitary units
spinde position
tub
Ncd

Figure S1

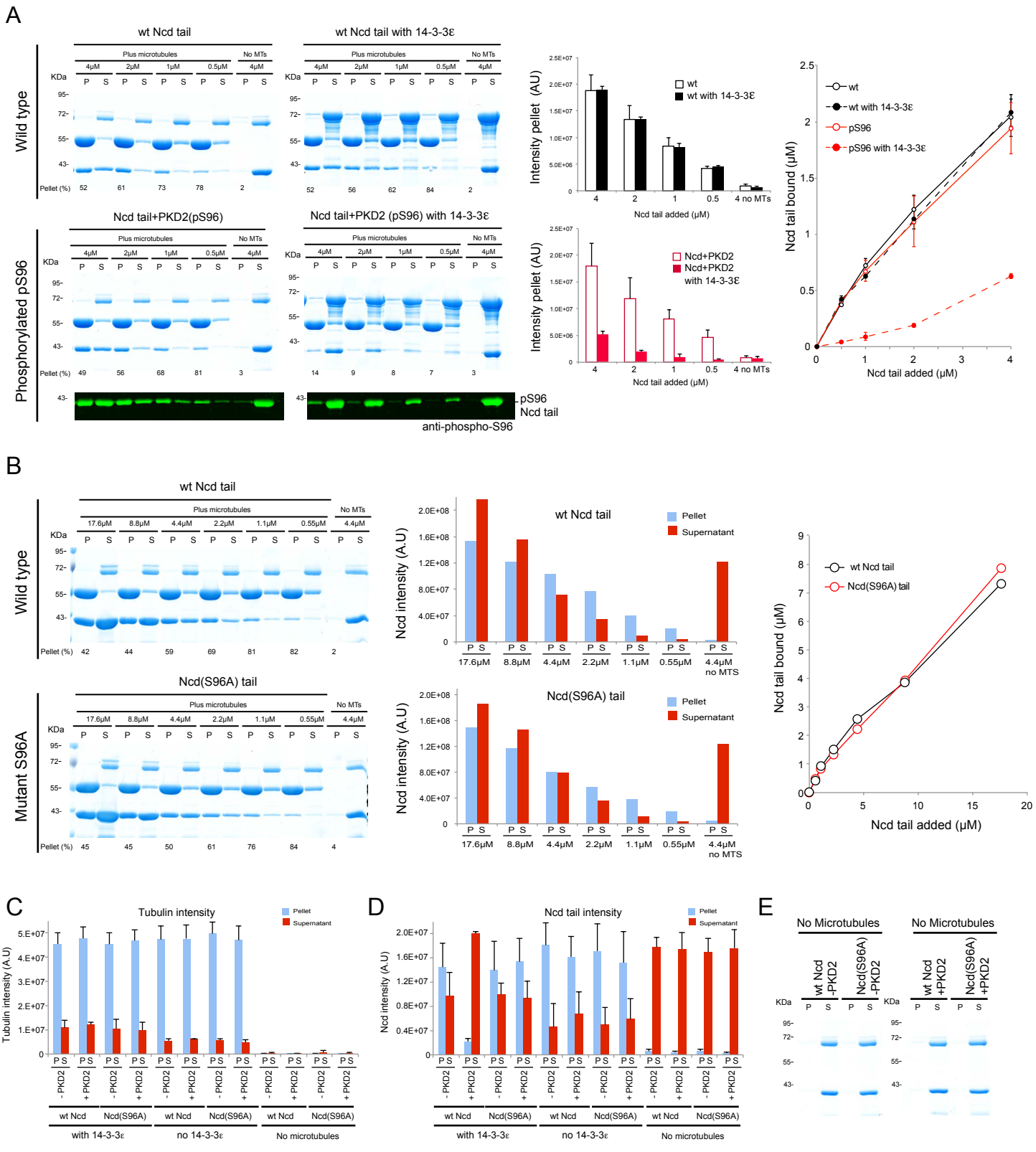
A
wt Ncd tail
wt Ncd tail with 14-3-3ε
Wild type
Plus microtubules
No MTs
4μM 2μM 1μM 0.5μM 4μM
KDa
P S
95-
72-
55-
43-
Pellet (%) 52 61 73 78 2
52 56 62 84 2
Ncd tail+PKD2(pS96)
Ncd tail+PKD2 (pS96) with 14-3-3ε
Phosphorylated pS96
Pellet (%) 49 56 68 81 3
14 9 8 7 3
Intensity pellet (AU)
wt
wt with 14-3-3ε
Ncd tail added (μM)
4 2 1 0.5 4 no MTs
Ncd+PKD2
Ncd+PKD2 with 14-3-3ε
Ncd tail bound (μM)
pS96
pS96 with 14-3-3ε
pS96
Ncd tail
anti-phospho-S96
B
wt Ncd tail
Wild type
17.6μM 8.8μM 4.4μM 2.2μM 1.1μM 0.55μM 4.4μM
Pellet (%) 42 44 59 69 81 82 2
Ncd(S96A) tail
Mutant S96A
Pellet (%) 45 45 50 61 76 84 4
Ncd intensity (A.U)
Pellet
Supernatant
17.6μM 8.8μM 4.4μM 2.2μM 1.1μM 0.55μM 4.4μM no MTS
wt Ncd tail
Ncd(S96A) tail
Ncd tail added (μM)
C
Tubulin intensity
Tubulin intensity (A.U)
- PKD2
+ PKD2
wt Ncd
Ncd(S96A)
with 14-3-3ε
no 14-3-3ε
No microtubules
D
Ncd tail intensity
E
No Microtubules
wt Ncd -PKD2
Ncd(S96A) -PKD2
wt Ncd +PKD2
Ncd(S96A) +PKD2

Figure S2

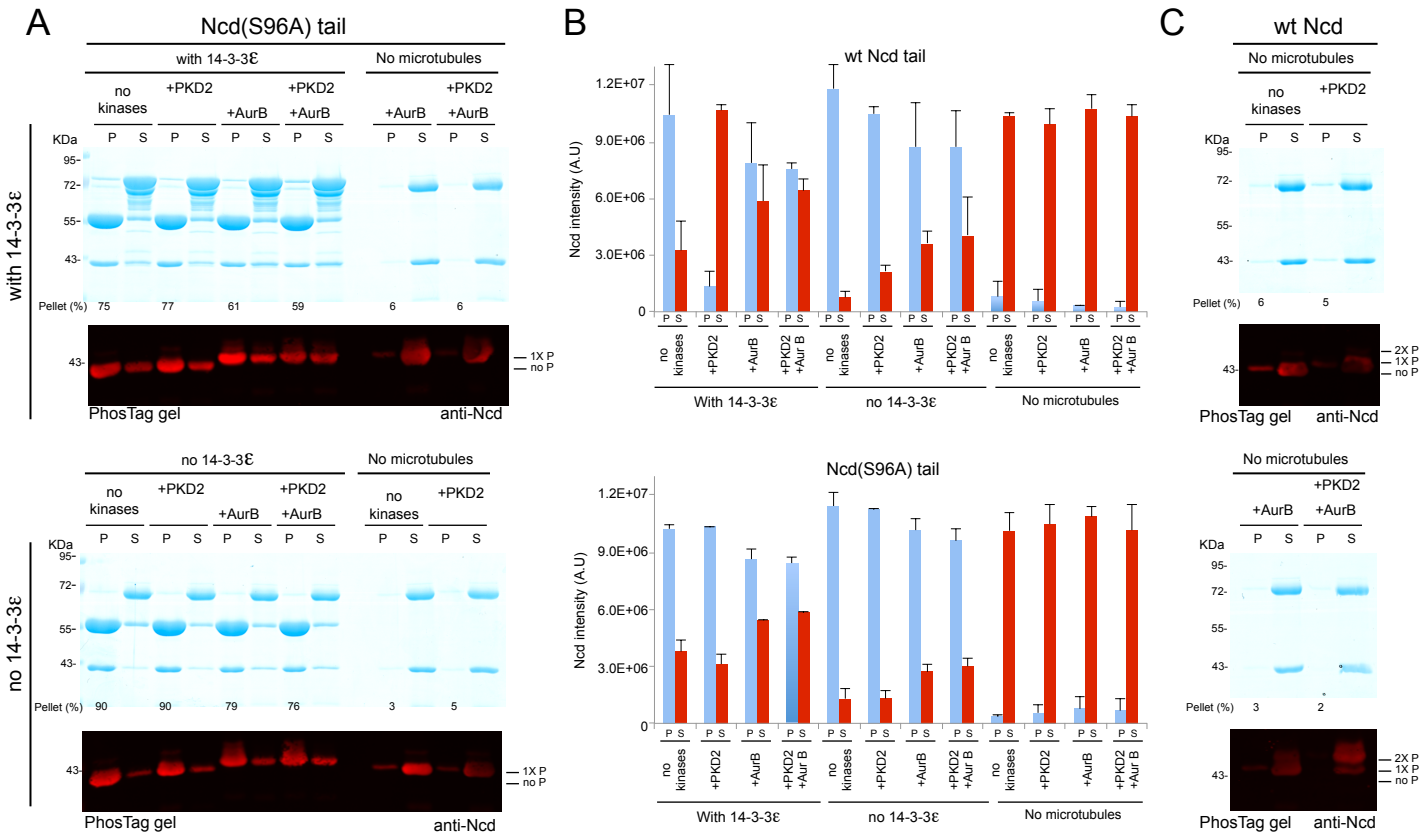
A
Ncd(S96A) tail
with 14-3-3ε
No microtubules
no kinases
+PKD2
+AurB
+PKD2 +AurB
KDa
P S
95-
72-
55-
43-
Pellet (%) 75 77 61 59 6 6
1X P
no P
PhosTag gel
anti-Ncd
with 14-3-3ε
no 14-3-3ε
Pellet (%) 90 90 79 76 3 5
B
wt Ncd tail
Ncd(S96A) tail
Ncd intensity (A.U)
1.2E+07
9.0E+06
6.0E+06
3.0E+06
0
no kinases
+PKD2
+AurB
+PKD2 +Aur B
With 14-3-3ε
no 14-3-3ε
No microtubules
C
wt Ncd
No microtubules
Pellet (%) 6 5
2X P
1X P
no P
PhosTag gel
anti-Ncd
Pellet (%) 3 2

Figure S3